AIMS Materials Science, 4(4): 956-969.
DOI: 10.3934/matersci.2017.4.956
Received: 30 June 2017
Accepted: 17 August 2017
Published: 29 August 2017

http://www.aimspress.com/journal/Materials

Research article

Conjugated polymers as functional hole selective layers in efficient metal halide perovskite solar cells

Silvia Colodrero *

Research group of Organic Nanostructured Photovoltaics, Institut de Ciencies Fotoniques (ICFO), The Barcelona Institute of Science and Technology, Av. Carl Friedrich Gauss 3, 08860 Castelldefels, Spain

*** Correspondence:** Email: silvia.colodrero@icfo.es; Tel: +34-935534122.

Abstract: Interface engineering is still an open question to be solved in the emerging field of metal halide perovskite solar cells. Although impressive advances have been already made in controlling the composition and the quality of the active layer, stability issues of complete devices are limiting yet the forefront of a future next generation of printable photovoltaics. At this point, the choice of proper charge selective layers is essential to yield perovskite solar cells with an optimal compromise between efficiency and stability. Even though diverse n-type materials displaying outstanding properties have been recently proposed, the record performances are yet limited to the use of p-type small molecule compounds with low hole mobility in their pristine form. In here, conjugated polymers widely used in the field of polymer solar cells are integrated in perovskite devices to behave as the hole selective layers. Apart from offering suitable hole mobility and energy matching with the valence band of the perovskite material to enable efficient charge extraction, their behaviour as potential functional barrier to protect the underlying perovskite film in standard n-i-p architectures is also discussed. Future work focused on developing novel alternatives based on more stable and efficient conjugated polymers might pave the way for the large scale production of perovskite solar cells.

Keywords: charge selective contacts; metal halide perovskite materials; conjugated polymers; efficiency; stability; recombination; photovoltaics

1. Introduction

In a short period of time metal halide perovskite (MHP) materials, with the general formula ABX_3, have revealed outstanding optoelectronic properties that make them uniquely suited for photovoltaic applications [1–4]. Along with their rapid development from liquid junction to solid state cells [5,6,7], the power conversion efficiency (PCE) was promoted from the initial 3.8% to recent values over 22% [8], thus standing close to nowadays inorganic thin film technologies [9]. A better control on the perovskite film morphology and composition through a large variety of solution processed techniques, together with an optimization of the device structure and interfaces, have allowed to a large extend such meteoric rise in efficiency [10–19]. However, there are still open questions regarding the role of the different interfaces present in the cell on the related charge processes that need to be further clarified.

MHP solar cells in planar configuration are strongly demanded at the forefront of a future next generation of printable photovoltaics [20]. In such case, the perovskite layer is sandwiched in between two charge transporting interlayers resulting in n-i-p or p-i-n like architectures [15]. Although they resemble in a way the configurations adopted by polymer solar cells (PSCs), the intrinsic characteristics of the perovskite layer are the ones governing the most the charge carrier lifetime and diffusion lengths [21–24]. On the other hand, electron and hole selective layers (ESLs and HSLs, respectively) are expected to fulfil the requirements to facilitate charge transport and to assist charge collection towards the respective electrodes, thus being essential in determining the final device performance [14,15]. Despite the mesoscopic TiO_2 n-i-p architectures have yielded the highest efficiencies reported so far [8,25,26], different metal oxide ESLs deposited as thin films have been proposed to simplify the device fabrication process. Among them, SnO_2 has recently demonstrated to be a promising choice due to its high electron mobility, wide band gap and long stability under UV illumination [27,28]. Also, ensembles based on a double ESL have been suggested to allow a more suitable energy band alignment with the conduction band of the perovskite material [29,30]. Similarly, although a great effort has been done on searching efficient HSL alternatives, small molecule type compounds, typically 2,2',7,7'-tetrakis(N,N-di-p-methoxyphenylamine)-9,9'-spirobifluorene (spiro-OMeTAD), have dominated the superior overall performances until now. However, their intrinsically low conductivity and the associated instability issues derived from the use of chemical dopants, which are added to increase the conductivity in presence of O_2, may compromise somehow the reproducibility and long term stability of the devices [31–36]. Besides, when the n-i-p architecture is considered, the HSL is sought to protect the quite sensitive absorber layer against the external humidity conditions by acting as a functional barrier [37,38,39]. Indeed, a variety of approaches has been also explored with the aim of hindering the moisture ingress through the top HSL [40–43].

Herein we evaluate and analyse the behaviour of different conjugated polymers when employed as the HSLs in planar perovskite solar cells designed with a typical n-i-p architecture. Such semiconducting polymers have been widely used in a variety of soft electronics, including PSCs, due to both their good film forming ability when processed through solution techniques and their unique and tuneable optical and electrical properties [44–47]. In spite of the high charge mobility they can exhibit in their pristine form, the parasitic absorption displayed over the visible range has restricted to a large extent their use in the context of perovskite solar cells [15]. However, several studies have already demonstrated that the morphology and crystallinity of such polymeric compounds can play a

crucial role on the efficacy of charge extraction and recombination and, therefore, on the final performance of the device [48–53]. In addition to an efficient charge generation and collection, raised open circuit voltage (Voc) values are also desired. Those will be mainly determined by the energy differences between the Fermi levels of the ESL and the HSL. For this reason, apart from revealing suitable hole mobility and chemical compatibility with the perovskite layer, another prerequisite to be accomplished by the HSL is that of a proper energy band alignment with the active layer. On the basis of such requirement, poly-3-hexylthiophene (P3HT) and poly([2,6'-4,8-di(5-ethylhexylthienyl)benzo[1,2-b;3,3-b]dithiophene] {3-fluoro-2[(2-ethylhexyl)carbonyl]thieno[3,4-b]thiophenediyl}) (PTB7-Th) are chosen herein as the hole transporting materials for planar perovskite solar cells. Those have demonstrated to give rise to optimal device performance when employed in bulk heterojunction PSCs [54,55]. Moreover, although P3HT has been explored in other research works within the field of perovskite solar cells, chemical dopants or more sophisticated approaches to tune its electrical properties have usually been employed to reach the best efficiency values [56,57,58]. In the present study, we pay attention to establish a possible correlation between the corresponding photovoltaic features and the dissimilar HSL properties for optimized devices yielding overall performances over 14%. Also, general aspects regarding the cell stability and the barrier protection provided by the different polymeric compounds will be discussed. To the best of our knowledge, no previous studies on the stability of the multilayer stacks or the complete devices have been carried out before when incorporating such kind of conducting polymers, free of additives, and under ambient conditions.

2. Materials and Methods

All commercially available chemicals were employed without any further purification. A 40 nm transparent film made of TiO_2 was first deposited by spin coating on top of the previously cleaned conductive fluorine tin oxide (FTO) substrates (8 Ω cm^{-2}, Pilkington®). To do so, a 0.25 M solution of titanium (IV) isopropoxide (TTIP 97%, Sigma Aldrich) in anhydrous ethanol (99.5%, Sharlau) was prepared by slowly adding the titanate precursor onto the alcoholic solvent while stirring. A final concentration of 0.02 M in hydrochloric acid (HCl 37%, Sigma Aldrich) was adjusted to avoid the precipitation of slurries during the preparation of the solution. A rotation speed of 3000 rpm was held during 40 seconds to give rise to the required thickness, the substrates being afterwards thermally annealed at 150 ℃ during 20 minutes and, subsequently, at 500 ℃ for 30 minutes. After cooling down, they were transferred to a N_2 glovebox for next fabrication steps. Similarly to the recipe reported by Lee at al. [7], the MHP precursor was prepared by dissolving methylammonium iodide (CH_3NH_3I 99.5%, 1-Material) and lead(II) chloride ($PbCl_2$ 98%, Sigma-Aldrich) in dimethylformamide (DMF 99.8%, Sigma-Aldrich) with a 3:1 molar ratio and a 32 wt% concentration. The perovskite solution was spin-coated on top of the ESL at 1500 rpm and the resulting films were annealed for 2 hours at 90 ℃ and 20 minutes at 125 ℃. For the HSL precursors, P3HT (4002-E, Rieke) and PTB7:Th (1-Material) solutions with a concentration of 15 mg/ml and 10 mg/ml, respectively, were prepared in anhydrous chlorobenzene (CB 99.8%, Sigma Aldrich) and kept under stirring overnight at 60 ℃ before using. They were also deposited by spin coating the respective solutions at a rotation speed of 2000 rpm during 45 seconds. Finally, an 80 nm thick gold top contact layer was evaporated in a high vacuum chamber (Lesker). The deposition rate was adjusted to 0.6 Å/s and a metal mask was place to define an active area of 0.096 cm^2.

The optical transmission of the different samples was measured over the wavelength range of interest using a UV-vis-NIR spectrometer (Lambda 950, PerkinElmer). Both the surface morphology and the cross section of the samples were evaluated by field emission scanning electron microscopy (FEG-SEM, FEI Inspect F50-EBL). The X-ray diffraction (XRD) patterns were recorded with a Bruker D8 Advance diffractometer (Bruker, Cu-Kα source). Film thickness values were checked employing a surface profilometer (KLA-Tencor Alpha-Step IQ Surface Profiler). The photovoltaic performance of the fabricated solar cells was determined using an AM 1.5G solar simulator (Sun 3000, Abet Technologies). The illumination intensity corresponding to 100 mW cm^{-2} was adjusted with a monocrystalline silicon reference cell (Hamamatsu) calibrated at the Fraunhofer Institute for Solar Energy Systems. The current density-voltage characteristics (JV) curves were then recorded by scanning voltages from negative to positive (forward) and from positive to negative (reverse) using a Keithley 2400 SourceMeter. EQE analysis was performed using a quantum efficiency measurement system (QEX10, PV Measurements). In this case, the devices were illuminated using a monochromatic light coming from a Xenon lamp. The spectral response of the calibrated silicon cell was used as a reference. All set of devices were tested under ambient conditions and without encapsulation.

3. Results and Discussion

The simplified molecular structures corresponding to the P3HT and PTB7:Th polymers to be used as HSLs can be found in Figure 1a. A scheme of the planar n-i-p device configuration proposed and the energy level diagram of the studied materials are also illustrated in Figures 1b–c.

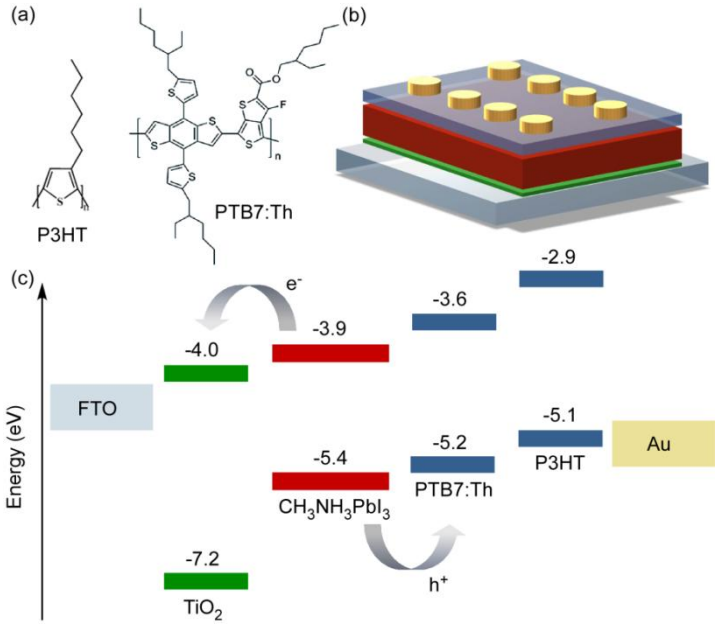

Figure 1. (a) Molecular structure of P3HT and PTB7:Th. (b)–(c) Scheme of the device configuration and energy level diagram of the studied materials, respectively.

As clearly seen, the MHP is sandwiched in between a thin and compact layer of TiO_2 and the HSL. FTO substrates and gold layers are used as the respective bottom and top contacts. The same

colour code for both the scheme and the diagram was used to identify each one of the layers composing the device. The energy levels for the different materials were extracted from the literature. From them, a proper alignment between the conduction bands of the ESL (TiO_2) and the perovskite is observed. Similarly, the highest occupied molecular orbitals (HOMO) energies suitably matched that of the perovskite valence band.

An optical characterization of both the perovskite and the HSL constituents was performed prior to the evaluation of the device performance. Figure 2a displays the absorbance measured for perovskite and polymeric films when deposited onto common glass substrates following the general procedure described in the Materials and methods section. While the MHP exhibits an absorption that is extended over the whole visible range, ranging from 350 to 760 nm, the conjugated polymers present narrower absorption bands centred at 530 nm and 700 nm for the P3HT and PTB7:Th, respectively. In principle, parasitic losses may be affecting the most in the case of PTB7:Th since its corresponding absorption takes place at a wavelength range in which the one resulting from the perovskite starts to decrease. However, by conventional optical spectroscopy, it is difficult to evaluate separately the contribution of useful and parasitic absorption in the polymeric compound since photoexcitation can generate charge carriers in both the perovskite and the HSLs. As shown in Figure 2b, the steady state photoluminescence measured when the perovskite film was excited with a 532 nm continuous wave laser coincides with the onset of absorption detected in the transmittance spectrum.

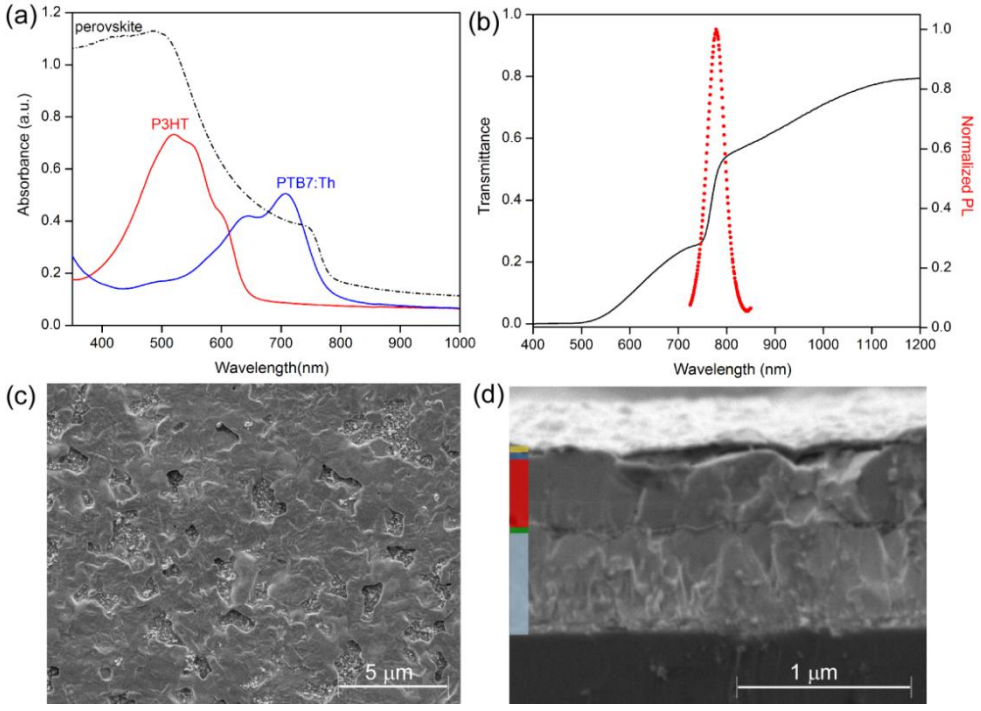

Figure 2. (a) Absorbance measured for perovskite (black dashed line), P3HT (red solid line) and PTB7:Th (blue solid line) films deposited onto glass substrates. (b) Transmittance spectrum (black line) and normalized photoluminescence (red circles) measured for the perovskite layer. (c)–(d) SEM images acquired from the perovskite layer top view and the cross section of a complete cell including P3HT as the HSL, respectively.

Figures 2c–d show SEM images taken from the top view of a perovskite layer and from the cross section of a complete cell in which P3HT was employed as the HSL. A long range interconnected and multi-faceted crystallites were observed from the top view image. Also, in spite of the special care taken during the crystallization process, large void spaces were formed into the films as a consequence of the removal of excess material during the thermal annealing step, as suggested elsewhere [11]. On the other hand, the continuous perovskite layer can be clearly appreciated from the cross section image, the thicknesses of the different layers being about 40 nm, 350 nm, 75 nm and 80 nm for the ESL, MHP, HSL and Au, respectively. Those were also double checked by using a surface profilometer.

The photovoltaic parameters extracted from the corresponding JV curves of complete devices integrating P3HT and PTB7:Th are compared in Figures 3a–d.

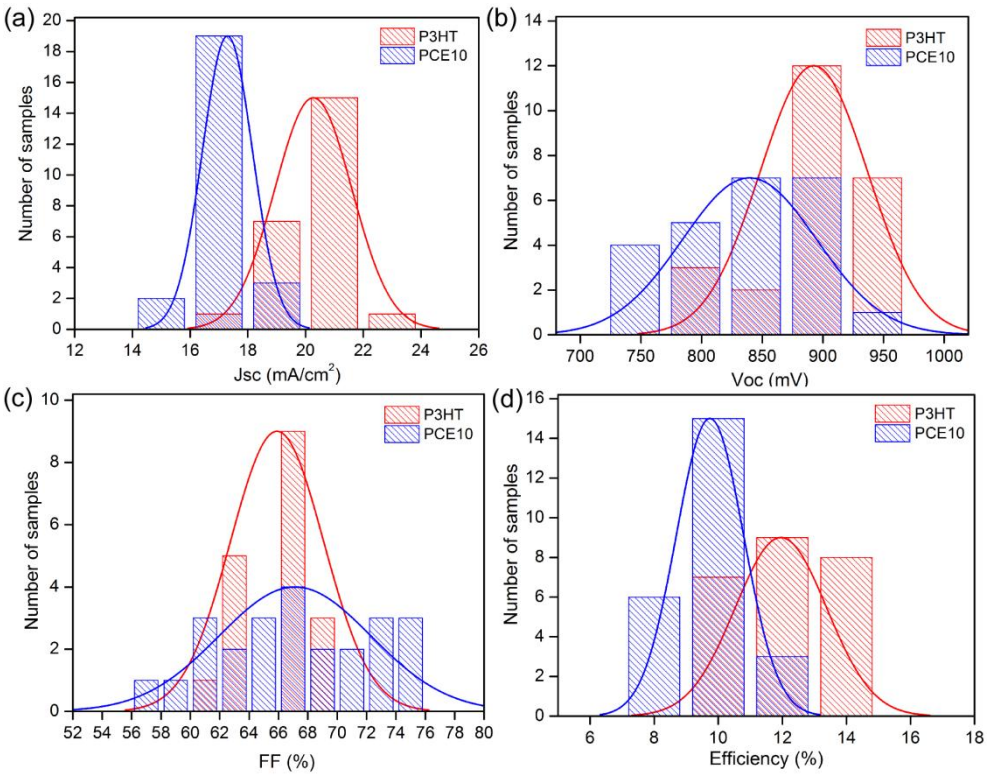

Figure 3. Comparison of histograms of photovoltaic parameters obtained for the perovskite solar cells based on P3HT (red) and PTB7:Th (blue).

Histogram plots are used to check the frequency distribution of each single variable dataset: the short circuit photocurrent density (Jsc), the open circuit photovoltage (Voc), the fill factor (FF) and the overall efficiency. For the analysis, a total of 24 samples were considered and the voltage scans were carried out from open circuit to short circuit conditions. As displayed in these graphs, higher Jsc and Voc were obtained for the case of devices based on P3HT as the HSL. Given that the FF values were similar in both cases, although with a narrower distribution for P3HT devices, the best device performances were still attained for perovskite solar cells integrating P3HT polymer. An average efficiency of about 12% was observed for P3HT based solar cells, which means an improvement of above 20% with respect to the average values achieved for the PTB7:Th ones. These

preliminary results suggest that, to sufficiently translate the deeper HOMO levels of conjugated polymers into higher Voc values, strategies for further improving and designing solution-processed interfacial materials should be taken into consideration.

Since the loss of photogenerated charge carriers can be associated to different recombination processes taking place within the device, a deeper insight into the possible factors or mechanisms determining the resulting photovoltaic characteristics is required. To probe the kinetics of charge carrier recombination, the JV curves were measured while the complete devices were illuminated over a range of light intensities going from 10 to 100 mW/cm^2. Representative perovskite solar cells displaying photovoltaic parameters over the average range were selected to carry out this study. In Figures 4a–b, the Jsc and Voc data are plotted on a log-log and linear-log scale, respectively. The Jsc-light intensity curves show a similar dependence for both the P3HT and PTB7:Th based devices. In this case, the curves were fitted according to the relation $Jsc \propto \Phi^{\alpha}$, where Φ corresponds to the light intensity and α to the exponent of the dependence. The factor α was calculated to be close to 1 in both cases, which implies that photocurrent is determined by the generation rate of electron–hole pairs due to photon absorption. The deviation from $\alpha = 1$ is typically attributed to bimolecular recombination or unbalanced charge transport of electrons and holes [59]. On the other hand, the light intensity dependence of Voc reveals the dominant recombination mechanism in the device as no external current is extracted under such conditions and all of the photogenerated charge carriers recombine. Slopes of kT/q and 2kT/q will indicate dominant bimolecular and trap-assisted recombination, respectively [60,61]. In here, a similar behaviour is also attained for both kinds of devices, a slope of ~2.3 kT/q being calculated. That means that trap assisted recombination is still the main recombination mechanism in perovskite solar cells. However, due to significant changes in the charge collection probability, which seems also to be dependent on the light intensity at a given applied voltage, bimolecular recombination cannot be completely disregarded. Although recombination channels can be present at the grain boundaries of the perovskite and at the interfaces, the latter has been conferred as the dominant loss mechanism [62,63,64]. Nonetheless, perovskite morphologies prepared under certain preparation methods might be more sensitive to the sign of traps, thus playing a crucial role on the final device performance and affecting the hysteretic behaviour of the cell.

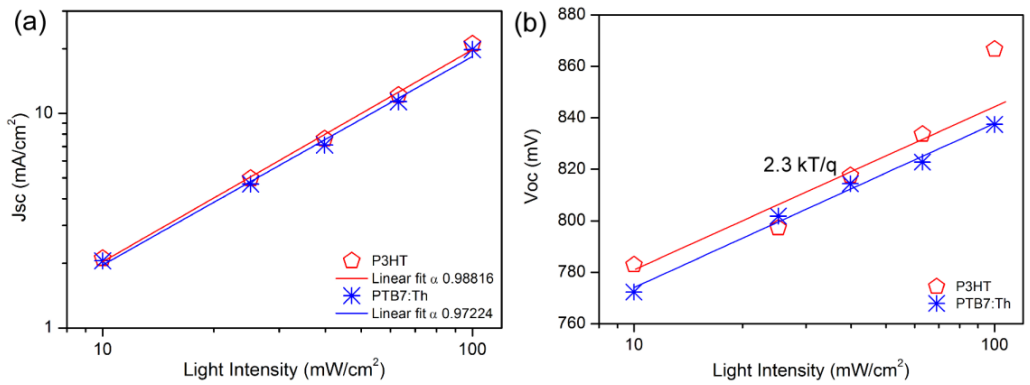

Figure 4. Light intensity dependence of (a) Jsc and (b) Voc for the perovskite solar cells integrating P3HT (red symbols) and PTB7:Th (blue symbols) as the HSLs. Solid lines represent the linear fittings in each case.

In order to investigate the hysteresis of the fabricated devices, the JV characteristics curves were sweeping from both forward and reverse directions. The results corresponding to the best performing cells are presented in Figure 5 and summarized in Table 1. All experimental data were collected without applying any preconditioning voltage to the cells. A slight hysteretic behaviour can be deduced from the graph, which affected mainly to the FF value of the devices while the Jsc and Voc were kept almost unaltered. This behaviour is more frequently shown in planar perovskite solar cells as a consequence of either the reduced contact area between the perovskite layer and the respective charge selective layers or the ineffective charge extraction of the latter. Although some studies have tried to correlate the density of traps and mobile ionic defects with the hysteretic behaviour [64], it is quite challenging yet the extrapolation to the large variety of perovskite morphologies, compositions and device configurations reported up to date.

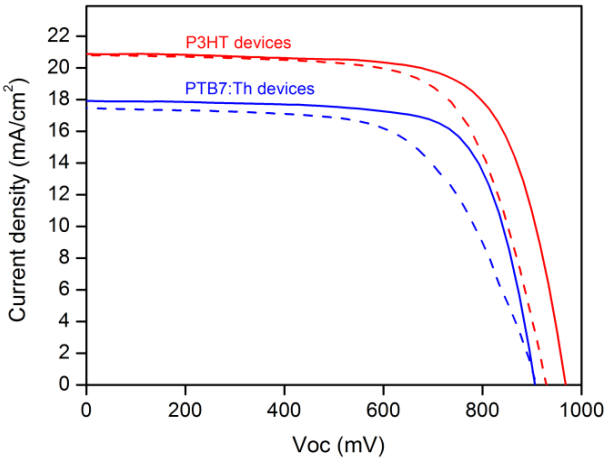

Figure 5. IV characteristics curves of the record efficiency cells measured for P3HT (red) and PTB7:Th (blue). Solid and dashed lines correspond to the reverse and forward scans, respectively.

Table 1. Summary of the photovoltaic parameters extracted from the IV curves presented in Figure 5 and measured for perovskite solar cells using P3HT and PTB7:Th under standard one sun illumination condition (100 mW/cm^2).

Device configuration	Jsc (mA/cm^2)	Voc (mV)	FF (%)	PCE (%)
FTO/TiO_2/MHP/P3HT/Au from OC to SC	20.9	968	71.4	14.4
FTO/TiO_2/MHP/P3HT/Au from SC to OC	20.8	929	68.2	13.2
FTO/TiO_2/MHP/PTB7:Th/Au from OC to SC	17.9	906	73.1	11.8
FTO/TiO_2/MHP/PTB7:Th/Au from SC to OC	17.5	906	63	10

As it can be clearly observed in Table 1, the perovskite solar cell based on P3HT displays PCE values of 14.4% and 13.2% when scanned in forward and reverse directions, respectively. In a similar way, that incorporating PTB7:Th as the HSL exhibits PCE values of 11.8% and 10% in the forward and reverse scans. As commented before, almost no changes in the Jsc and Voc were observed, while the reduction in the FF value was around 4.5% and 14% for the case of perovskite solar cells incorporating P3HT and PTB7:Th. It means that around 92% and 85% of the efficiency values measured under reverse scan were maintained for the forward sweep in both kinds of devices.

Finally, in order to address the stability issue of perovskite solar cells, a preliminary study of the barrier properties offered by the two conjugated polymers was carried out by means of optical measurements. Although no evidence of degradation after prolonged time exposures was noticed during the photovoltaic characterization of the complete devices (Figure S1 in the Supplementary section), such test could be employed as a quick tool to evaluate the stability of individual and stacked layers under stressed conditions (light, temperature and H_2O). To do so, the samples were kept under continuous illumination at 1 sun while the corresponding optical properties were check at certain time intervals (every 1 hour in this experiment). Since the final goal was to identify any degradation signal over the visible spectral range, those were constructed onto common glass substrates following the proposed n-i-p architecture and without depositing the top metallic layer. A schematic drawing of the samples under 1 sun illumination is depicted in Figure 6a, and the results extracted from this analysis are presented in Figures 6b–f.

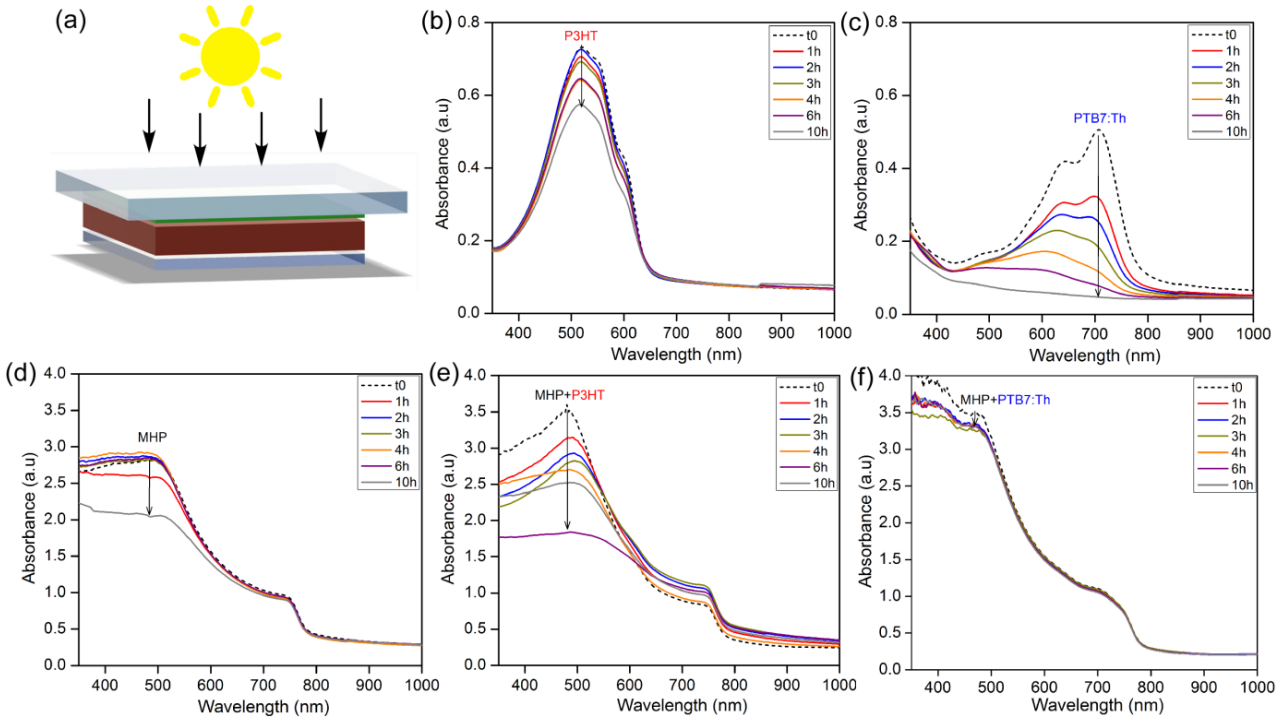

Figure 6. (a) Schematic drawing of samples under illumination. (b)–(f) Evolution of the optical response versus the illumination time for purely polymeric films and the n-i-p architectures.

No UV filters were employed during the illumination of samples and the humidity in the laboratory was around 40%. Those are key parameters that can determine the kinetics of deterioration in polymeric and perovskite materials. Figures 6b–c show the clear degradation of the different polymeric compounds under simulated sunlight illumination conditions. Whereas P3HT still preserved its optical features after 10 hours of continuous illumination, PTB7:Th became almost transparent over the visible, with no apparent absorbance after this time. However, when the perovskite layer was considered, the sample covered by PTB7:Th surprisingly kept (Figure 6f) the same response after the 10 hour illumination time. It might be explained due to the synergy of both the perovskite and the PTB7:Th films, the former blocking the UV radiation to reach the polymeric material and the latter behaving as an effective barrier protection to avoid the ingress of moisture. On the other hand, the most significant change detected in the bare and P3HT coated perovskite films was located at the spectral range comprised between 350 nm and 600 nm, as shown in Figures 6d–e.

4. Conclusions

The results presented in this work show the potential that different conjugated polymers can have when performing as HSLs in perovskite solar cells. P3HT and PTB7:Th based devices were herein evaluated to establish a possible correlation between the photovoltaic performance and the respective optical and electrical properties conferred by the polymeric material. Although parasitic losses seem to be affecting the most in the case of perovskite solar cells integrating PTB7:Th as the HSL, recombination kinetics extracted from the light intensity dependence of Voc reveal the same behaviour in both types of devices, with a trap assisted recombination being the main loss mechanism. Even though, performances of around 14% and 12% in reverse voltage scans, or 13% and 10% in forward scans, were reached for pristine P3HT and PTB7:Th based solar cells, respectively. Since chemical additive free polymers are desired for long term stability cells, this study opens the door for a conscious and rational optimization of the electrical and optical properties of polymeric compounds to yield perovskite solar cells with an optimal compromise between efficiency and stability.

Acknowledgments

This research was carried out at ICFO with financial support from the Spanish MINECO (Severo Ochoa program, grant No.: SEV-2015-0522), the MINECO and the Fondo Europeo de Desarrollo Regional FEDER (grant No.: MAT2014-52985-R), the Fundació Privada Cellex, and from the EC FP7 Program (ICT-2011.35) under grant agreement n NMP3-SL-2013-604506. The author thanks the collaboration of Dr. Miguel Montes-Bajo for his assistance with the structural characterization of the samples presented in this paper.

Conflict of Interest

The author declares no conflicts of interest in this paper.

References

1. Sum TC, Mathews N (2014) Advancements in perovskite solar cells: photophysics behind the photovoltaics. *Energ Environ Sci* 7: 2518–2534.
2. Stoumpos CC, Kanatzidis MG (2015) The renaissance of halide perovskites and their evolution as emerging semiconductors. *Accounts Chem Res* 48: 2791–2802.
3. Chen Q, De Marco N, Yang Y, et al. (2015) Under the spotlight: The organic-inorganic hybrid halide perovskite for optoelectronic applications. *Nano Today* 10: 355–396.
4. Zhao Y, Zhu K (2016) Organic-inorganic hybrid lead halide perovskites for optoelectronic and electronic applications. *Chem Soc Rev* 45: 655–689.
5. Kojima A, Teshima K, Shirai Y, et al. (2009) Organometal halide perovskites as visible-light sensitizers for photovoltaic cells. *J Am Chem Soc* 131: 6050–6051.
6. Kim HS, Lee CR, Im JH, et al. (2012) Lead iodide perovskite sensitized all-solid-state submicron thin film mesoscopic solar cell with efficiency exceeding 9%. *Sci Rep* 2: 591.
7. Lee MM, Teuscher J, Miyasaka T, et al. (2012) Efficient hybrid solar cells based on meso-superstructured organometal halide perovskites. *Science* 338: 643–647.
8. Saliba M, Matsui T, Domanski K, et al. (2016) Incorporation of rubidium cations into perovskite solar cells improves photovoltaic performance. *Science* 354: 206–209.
9. Green MA, Emery K, Hishikawa Y, et al. (2014) Solar cell efficiency tables (Version 45). *Prog Photovolt Res Appl* 23: 1–9.
10. Burschka J, Pellet N, Moon SJ, et al. (2013) Sequential deposition as a route to high-performance perovskite-sensitized solar cells. *Nature* 499: 316–319.
11. Eperon GE, Burlakov VM, Docampo P, et al. (2014) Morphological control for high performance, solution-processed planar heterojunction perovskite solar cells. *Adv Funct Mater* 24: 151–157.
12. Liang PW, Liao CY, Chueh CC, et al. (2014) Additive enhanced crystallization of solution-processed perovskite for highly efficient planar-heterojunction solar cells. *Adv Mater* 26: 3748–3754.
13. Xie FX, Zhang D, Su H, et al. (2015) Vacuum-assisted thermal annealing of $CH_3NH_3PbI_3$ for highly stable and efficient perovskite solar cells. *ACS Nano* 9: 639–646.
14. Zuo L, Gu Z, Ye T, et al. (2015) Enhanced photovoltaic performance of $CH_3NH_3PbI_3$ perovskite solar cells through interfacial engineering using self-assembling monolayer. *J Am Chem Soc* 137: 2674–2679.
15. Seo J, Noh JH, Seok Sl (2016) Rational strategies for efficient perovskite solar cells. *Accounts Chem Res* 49: 562–572.
16. Eperon GE, Stranks SD, Menelaou C, et al. (2014) Formamidinium lead trihalide: a broadly tunable perovskite for efficient planar heterojunction solar cells. *Energ Environ Sci* 7: 982–988.
17. Xiao Z, Dong Q, Bi C, et al. (2014) Solvent annealing of perovskite-induced crystal growth for photovoltaic-device efficiency enhancement. *Adv Mater* 26: 6503–6509.
18. Long M, Zhang T, Xu W, et al. (2017) Large-grain formamidinium $PbI_{3-x}Br_x$ for high-performance perovskite solar cells via intermediate halide exchange. *Adv Energy Mater* 7: 1601882.
19. Long M, Zhang T, Zhu H, et al. (2017) Textured $CH_3NH_3PbI_3$ thin film with enhanced stability for high performance perovskite solar cells. *Nano Energy* 33: 485–496.

20. Williams ST, Rajagopal A, Chueh CC, et al. (2016) Current challenges and prospective research for upscaling hybrid perovskite photovoltaics. *J Phys Chem Lett* 7: 811–819.
21. Stranks SD, Eperon GE, Grancini G, et al. (2013) Electron-hole diffusion lengths exceeding 1 micrometer in an organometal trihalide perovskite absorber. *Science* 342: 341–344.
22. Xing G, Mathews N, Sun S, et al. (2013) Long-range balanced electron- and hole-transport lengths in organic-inorganic $CH_3NH_3PbI_3$. *Science* 342: 344–347.
23. Shi D, Adinolfi V, Comin R, et al. (2015) Low trap-state density and long carrier diffusion in organolead trihalide perovskite single crystals. *Science* 347: 519–522.
24. De Quilettes DW, Vorpahl SM, Stranks SD, et al. (2015) Impact of microstructure on local carrier lifetime in perovskite solar cells. *Science* 348: 683–686.
25. Yang WS, Noh JH, Jeon NJ, et al. (2015) High-performance photovoltaic perovskite layers fabricated through intramolecular exchange. *Science* 348: 1234–1237.
26. Jeon NJ, Noh JH, Yang WS, et al. (2015) Compositional engineering of perovskite materials for high-performance solar cells. *Nature* 517: 476–480.
27. Ke W, Fang G, Liu Q, et al. (2015) Low-temperature solution-processed tin oxide as an alternative electron transporting layer for efficient perovskite solar cells. *J Am Chem Soc* 137: 6730–6733.
28. Anaraki EH, Kermanpur A, Steier L, et al. (2016) Highly efficient and stable planar perovskite solar cells by solution-processed tin oxide. *Energ Environ Sci* 9: 3128–3134.
29. Xu X, Zhang H, Shi J, et al. (2015) Highly efficient planar perovskite solar cells with a TiO_2/ZnO electron transport bilayer. *J Mater Chem A* 3: 19288–19293.
30. Okamoto Y, Suzuki Y (2016) Mesoporous $BaTiO_3/TiO_2$ double layer for electron transport in perovskite solar cells. *J Phys Chem C* 120: 13995–14000.
31. Nguyen WH, Bailie CD, Unger EL, et al. (2014) Enhancing the hole-conductivity of spiro-OMeTAD without oxygen or lithium salts by using spiro$(TFSI)_2$ in perovskite and dye-sensitized solar cells. *J Am Chem Soc* 136: 10996–11001.
32. Kim HS, Seo JY, Park NG (2016) Impact of selective contacts on long-term stability of $CH_3NH_3PbI_3$ perovskite solar cells. *J Phys Chem C* 120: 27840–27848.
33. Liu Y, Chen Q, Duan HS, et al. (2015) A dopant-free organic hole transport material for efficient planar heterojunction perovskite solar cells. *J Mater Chem A* 3: 11940–11947.
34. Xu J, Voznyy O, Comin R, et al. (2016) Crosslinked remote-doped hole-extracting contacts enhance stability under accelerated lifetime testing in perovskite solar cells. *Adv Mater* 28: 2807–2815.
35. Kim GW, Kang G, Kim J, et al. (2016) Dopant-free polymeric hole transport materials for highly efficient and stable perovskite solar cells. *Energ Environ Sci* 9: 2326–2333.
36. Habisreutinger SN, McMeekin DP, Snaith HJ, et al. (2016) Research Update: Strategies for improving the stability of perovskite solar cells. *APL Mater* 4: 091503.
37. Yang J, Siempelkamp BD, Liu D, et al. (2015) Investigation of $CH_3NH_3PbI_3$ degradation rates and mechanisms in controlled humidity environments using in situ techniques. *ACS Nano* 9: 1955–1963.
38. Christians JA, Miranda Herrera PA, Kamat PV (2015) Transformation of the excited state and photovoltaic efficiency of $CH_3NH_3PbI_3$ perovskite upon controlled exposure to humidified air. *J Am Chem Soc* 137: 1530–1538.

39. Leguy AMA, Hu Y, Campoy-Quiles M, et al. (2015) Reversible Hydration of $CH_3NH_3PbI_3$ in Films, Single Crystals, and Solar Cells. *Chem Mater* 27: 3397–3407.
40. Habisreutinger SN, Leijtens T, Eperon GE, et al. (2014) Carbon nanotube/polymer composites as a highly stable hole collection layer in perovskite solar cells. *Nano Lett* 14: 5561–5568.
41. Smith IC, Hoke ET, Solis-Ibarra D, et al. (2014) A layered hybrid perovskite solar-cell absorber with enhanced moisture stability. *Angew Chem* 126: 11414–11417.
42. Leijtens T, Giovenzana T, Habisreutinger SN, et al. (2016) Hydrophobic organic hole transporters for improved moisture resistance in metal halide perovskite solar cells. *ACS Appl Mater Interfaces* 8: 5981–5989.
43. Hwang I, Jeong I, Lee J, et al. (2015) Enhancing stability of perovskite solar cells to moisture by the facile hydrophobic passivation. *ACS Appl Mater Interfaces* 7: 17330–17336.
44. Sirringhaus H, Tessler N, Friend RH (1998) Integrated optoelectronic devices based on conjugated polymers. *Science* 280: 1741–1744.
45. Pei Q, Yu G, Zhang C, et al. (1995) Polymer light-emitting electrochemical cells. *Science* 269: 1086–1088.
46. Yu G, Gao J, Hummelen JC, et al. (1995) Polymer photovoltaic cells: enhanced efficiencies via a network of internal donor–acceptor heterojunctions. *Science* 270: 1789–1791.
47. Forrest SR (2004) The path to ubiquitous and low-cost organic electronic appliances on plastic. *Nature* 428: 911–918.
48. Bi D, Yang L, Boschloo G, et al. (2013) Effect of different hole transport materials on recombination in $CH_3NH_3PbI_3$ perovskite-sensitized mesoscopic solar cells. *J Phys Chem Lett* 4: 1532–1536.
49. Heo JH, Im SH, Noh JH, et al. (2013) Efficient inorganic-organic hybrid heterojunction solar cells containing perovskite compound and polymeric hole conductors. *Nat Photonics* 7: 486–491.
50. Kwon YS, Lim J, Yun HJ, et al. (2014) A diketopyrrolopyrrole-containing hole transporting conjugated polymer for use in efficient stable organic-inorganic hybrid solar cells based on a perovskite. *Energ Environ Sci* 7: 1454–1460.
51. Zhu Z, Bai Y, Lee HK, et al. (2014) Polyfluorene derivatives are high-performance organic hole-transporting materials for inorganic-organic hybrid perovskite solar cells. *Adv Funct Mater* 24: 7357–7365.
52. Kranthiraja K, Gunasekar K, Kim H, et al. (2017) High-performance long-term-stable dopant-free perovskite solar cells and additive-free organic solar cells by employing newly designed multirole π-conjugated polymers. *Adv Mater* 29: 1700183.
53. Long M, Chen Z, Zhang T, et al. (2016) Ultrathin efficient perovskite solar cells employing a periodic structure of a composite hole conductor for elevated plasmonic light harvesting and hole collection. *Nanoscale* 8: 6290–6299.
54. He Z, Xiao B, Liu F, et al. (2015) Single-junction polymer solar cells with high efficiency and photovoltage. *Nat Photonics* 9: 174–179.
55. Chen D, Nakahara A, Wei D, et al. (2011) P3HT/PCBM bulk heterojunction organic photovoltaics: correlating efficiency and morphology. *Nano Lett* 11: 561–567.
56. Di Giacomo F, Razza S, Matteocci F, et al. (2014) High efficiency $CH_3NH_3PbI_{(3-x)}Cl_x$, perovskite solar cells with poly(3-hexylthiophene) hole transport layer. *J Power Sources* 251: 152–156.

57. Xiao JY, Shi JJ, Liu HB, et al. (2015) Efficient $CH_3NH_3PbI_3$ perovskite solar cells based on graphdiyne (GD)-modified P3HT hole-transporting material. *Adv Energy Mater* 5: 1401943.
58. Guo YL, Liu C, Inoue K, et al. (2014) Enhancement in the efficiency of an organic-inorganic hybrid solar cell with a doped P3HT hole-transporting layer on a void-free perovskite active layer. *J Mater Chem A* 2: 13827–13830.
59. Zhao N, Osedach TP, Chang LY, et al. (2010) Colloidal PbS quantum dot solar cells with high fill factor. *ACS Nano* 4: 3743–3752.
60. Koster LJA, Mihailetchi VD, Ramaker R, et al. (2005) Light intensity dependence of open-circuit voltage of polymer: fullerene solar cells. *Appl Phys Lett* 86: 123509–123509.
61. Mandoc M, Kooistra F, Hummelen J, et al. (2007) Effect of traps on the performance of bulk heterojunction organic solar cells. *Appl Phys Lett* 91: 263505.
62. Wetzelaer GAH, Scheepers M, Sempere AM, et al. (2015) Trap-assisted non-radiative recombination in organic-inorganic perovskite solar cells. *Adv Mater* 27: 1837–1841.
63. Sherkar TS, Momblona C, Gil-Escrig L, et al. (2017) Improving the performance of perovskite solar cells: insights from a validated device model. *Adv Energy Mater* 7: 1602432.
64. Sherkar TS, Momblona, C, Gil-Escrig L, et al. (2017) Recombination in perovskite solar cells: significance of grain boundaries, interface traps, and defect ions. *ACS Energy Lett* 2: 1214–1222.

AIMS Press